Atomic Spectroscopy

Article

# Novel Magnetic Ion-imprinted Polymer Extraction of Trace Ce(III) in Environmental and Mineral Samples and Determination by ICP-MS

Yu Hua,[a] Sen Zhang,[a] Hong Min,[b] Jia-yuan Li,[a] Xiao-hong Wu,[b] Dong Sheng,[a] Xiao-bing Cui,[c] Yi-jun Chen,[a] Chen Li,[b] Hong-zhen Lian[a,*] and Shu Liu [b,*]

[a] State Key Laboratory of Analytical Chemistry for Life Science, School of Chemistry & Chemical Engineering and Center of Materials Analysis, Nanjing University, Nanjing 210023, P. R. China

[b] Technical Center for Industrial Product and Raw Material Inspection and Testing, Shanghai Customs, Shanghai 200135, P. R. China

[c] College of Pharmacy, Nanjing University of Chinese Medicine, Nanjing 210023, P. R. China

***Received:*** *April 04, 2021;* ***Revised:*** *May 18, 2021;* ***Accepted:*** *May 20, 2021;* ***Available online:*** *May 24, 2021.*

***DOI: 10.46770/AS.2021.027***

**ABSTRACT:** A novel magnetic Ce(III) ion-imprinted polymer (Ce(III)-MIIP), grafted on organic-inorganic hybrid monolithic vinyl functionalized $Fe_3O_4$ ($Fe_3O_4$@HM), was synthesized for the first time by using the surface ion imprinting technology, in which Ce(III) was used as the template ion and acrylamide as the functional monomer. After the synthesized nanocomposites were well characterized, some parameters such as pH, adsorption time, eluent type, elution time and eluent volume, which affects the efficiency of magnetic solid phase extraction (MSPE), were studied in the determination of Ce(III). Under the optimized experimental conditions, Ce(III)-MIIP nanoparticles were used as the MSPE matrix, followed by inductively coupled plasma mass spectrometry (ICP-MS) determination with excellent selectivity, strong anti-interference ability, low mass transfer resistance and high adsorption capacity. The limit of detection, enrichment factor and adsorption capacity were 0.008 $\mu g \cdot L^{-1}$, 25 and 67.8 $mg \cdot g^{-1}$, respectively. The protocol was validated by analyzing certified reference materials and spike recoveries of complex environmental and mineral samples with satisfactory results. The relative standard deviations for the real samples were 1.7%~7.0%. In view of the advantages of facile preparation, fast adsorption rate, excellent selectivity and high adsorption capacity to Ce(III), the hybrid monolith-assisted Ce(III)-MIIP-based MSPE-ICP-MS protocol is promising for the determination of cerium in real environmental and mineral samples.

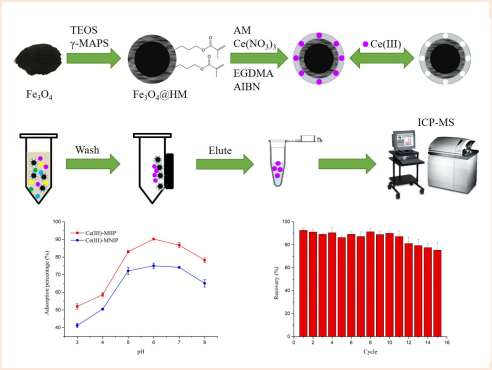


## INTRODUCTION

Rare earth elements (REEs) are widely used in industrial fields due to their optical and electrical properties.[1, 2] As a rare earth metal element with the highest abundance in nature, cerium plays an important role in lighting, biological medicine and ceramics,[3, 4] and is also an important part of many products, such as automotive catalytic converters, diesel additives and plant growth regulators.[5, 6] Moreover, cerium in some mineral samples can indicate its origin and provide valuable information in traceability of origin,[7] while the cerium content of particulate matter (PM) in some specific areas can provide valuable information about environmental sources.[8] However, cerium usually leads to accumulated toxicity, and with the increasing use of cerium-containing products, the possibility of its release into the environment is also increasing. It can accumulate in the body through the food chain, which will cause potential harm to human health.[9] Therefore, it is critical to determine cerium in environmental and mineral samples.

Many techniques have been reported for the determination of cerium, such as inductively coupled plasma mass spectrometry (ICP-MS),[10,11] inductively coupled plasma optical emission spectrometry (ICP-OES),[12, 13] X-ray fluorescence spectrometry,[14,15] *etc.* ICP-MS has the advantages of high

sensitivity, wide dynamic linear range, multi-element ability, *etc.*, making it the most powerful detection technology for trace element analysis. However, the existing level of cerium in the majority of real samples with complex matrices is lower than the limit of detection (LOD) of ICP-MS. This causes serious matrix effects and makes it difficult to get accurate analysis results with direct measuring methods. Especially metal ores with a high main metal content can cause instrumental contamination or even damage. In order to solve these problems, a pre-concentration step before analysis is required. Therefore, developing a suitable pretreatment method with perfect selectivity and high sensitivity for the determination of cerium in environmental and mineral samples is of great significance.

Combined with the above cerium detection technologies, there are a variety of separation and enrichment methods, including ion-exchange,[16, 17] solid phase extraction (SPE)[18] and liquid-liquid extraction,[19] among which SPE plays an important role due to its efficiency, simplicity and flexibility. SPE is one of the commonly used pretreatment methods for trace metal ions with the advantages of strong separation ability, high enrichment coefficient, less sample and solvent consumption, *etc.* As one of the latest SPE methods, magnetic solid phase extraction (MSPE) has attracted widespread attention because no centrifugation and/or filtration are needed after extraction with magnetic nanoparticles (MNPs) when the static batch mode is applied. The whole operating process is more convenient and time-saving than ordinary SPE.[20] However, the main problem with MSPE is that most of the existing adsorbents, usually functionalized nanoparticles, are non-specific and do not have sufficient selectivity for certain metal ions.[21] The presence of a large number of coexisting elements is not conducive to the extraction of target ions from the solution, and matrix interference will affect the accuracy of subsequent ICP-MS analysis. Thus, it is critical to develop a novel adsorbent with high selectivity and adsorption capacity.

L Recently, ion-imprinted polymers (IIPs) have received extensive attention because of their specific recognition to target ions.[22] Ion imprinting is a process where cross-linking functional monomers are aligned in a predetermined orientation to their stereo-chemical interactions with the template ions. Template ions and functional monomers are mainly combined through non-covalent bonds, including hydrogen bonds, ionic bonds, Van der Waals forces, *etc.*[23] In addition, some functional monomers can be combined with the target ions through coordination, and the resulting IIPs have more stable binding sites and better selectivity for target ions.[24] The high selectivity of IIPs can be explained by the polymer memory effect toward the metal ions related to the coordination geometry, coordination number, *etc.*

Currently, different approaches have been reported for metal ion imprinted polymers, such as bulk polymerization,[25] precipitation polymerization,[26] suspension polymerization[27] and so on. Keçili *et al.*[28] developed a novel Ce(III) ion imprinted cryogel-based bulk polymerization technique in which 2-hydroxyethyl methacrylate (HEMA) and N-methacryloylamido antipyrine (MAAP) were used as functional monomers. The prepared cryogels were successfully applied for the selective extraction of Ce(III) ions from aqueous solutions and bastnasite ore samples. Although these methods possess the advantage of high selectivity, they suffer some disadvantages, such as heterogeneous distribution of the binding sites, embedding of most binding sites, slow mass transfer rate and incomplete removal of the templates. To overcome the above shortcomings, the surface ion imprinting technology has received wide attention due to its complete template removal, low mass transfer resistance, good site accessibility for target ions, large adsorption capacity and simple preparation.[29-31] Zhang *et al.*[32] prepared a Ce(III)-imprinted functionalized potassium tetratitanate whisker adsorbent by using the surface-imprinting technique with chitosan as the functional monomer. Pan *et al.*[33] established a surface-imprinting technique combined with a sacrificial support process to synthesize a Ce(III)-imprinted polymer in which attapulgite acted as the sacrificial support material. These two methods were applied to the separation and determination of trace Ce(III) in river sediments combined with inductively coupled plasma-atomic emission spectrometry (ICP-AES). However, there is a very complicated post-process following the SPE procedure, such as requiring filtration and centrifugation when applying these IIPs. Therefore, it is urgent to develop new IIPs with a simple separation process. Furthermore, if IIPs encapsulating $Fe_3O_4$ as nuclear can be synthesized, the magnetic separation will replace the filtration and centrifugation steps in a convenient and economical way. Liu *et al.*[34] have synthesized a Ce(III)-IIP grafted on $Fe_3O_4$ nanoparticles supported by SBA-15 mesoporous microreactor via reversible addition-fragmentation chain transfer (RAFT) polymerization for the selective removal of Ce(III) from aqueous solution. Ce(III) was combined with the functional monomer acrylamide (AM) by coordination bonds, and the competitive adsorption studies showed that Ce(III)-IIP offered the advantages of selectivity towards Ce(III) compared with a non-imprinted polymer (NIP) in the presence of other metal ions. However, the multistep preparation contained magnetic SBA-15 (m-SBA-15), m-SBA-15@Cl, m-SBA-15@RAFT and finally a coating m-SBA-15@RAFT with the Ce(III)-imprinted layer. Some post-modification reactions were carried out for organic solvents but they are very time-consuming.

Our previous work[35] was based on the solvothermal method for generating $Fe_3O_4$ nanoparticles and the "one-pot" method for synthesizing organic-inorganic hybrid monolithic vinyl functionalized $Fe_3O_4$ ($Fe_3O_4$@HM) of good chemical and mechanical stability. In the present study, a magnetic Ce(III) ion-imprinted polymer (Ce(III)-MIIP) was synthesized, during which Ce(III) was used as the template ions, and AM, ethylene glycol

dimethacrylate (EGDMA) and 2,2'-azobisisobutyronitrile (AIBN) were used as the functional monomer, cross-linking agent and initiator, respectively. After characterization, the adsorption condition on the Ce(III)-MIIP and the elution condition from the Ce(III)-MIIP of the cerium ions were optimized. Finally, the application potential of Ce(III)-MIIP was investigated as MSPE absorbent for the ICP-MS determination of Ce(III) in environmental waters, sediments, soils, atmospheric particles, coals and iron ores.

## EXPERIMENTAL

**Reagents and materials.** All reagents used in the following experiments were of analytical reagent grade, unless otherwise stated. Ferric trichloride ($FeCl_3·6H_2O$), anhydrous sodium acetate ($CH_3COONa$), ethylene glycol (EG), HCl, $NH_3·H_2O$ (25%), methanol and ethanol were purchased from Nanjing Chemical Reagent Company (Nanjing, P. R. China). Tetraethoxysilane (TEOS) and methacryloxy propyl trimethoxyl silane (γ-MAPS) were from Alfa Aesar (Tianjin, P. R. China). Acrylamide (AM) and cerium nitrate ($Ce(NO_3)_3·6H_2O$) were from Macklin Biochemical Technology Co. Ltd. (Shanghai, P. R. China). Ethylene glycol dimethacrylate (EGDMA) and 2,2'-azobisisobutyronitrile (AIBN) were from Aladdin Biological Technology Co. Ltd. (Shanghai, P. R. China). Pure water (18.25 MΩ·cm) obtained from a Milli-Q water system (Millipore, Bedford, MA, USA) was used throughout the experiment.

In this paper, different kinds of environmental and mineral samples were selected to evaluate the analytical performance of the protocol. Certified reference materials GBW07403 soil sample (GSS-3) and GBW07310 sediment sample (GSD-10) were purchased from the Institute of Geophysical and Geochemical Prospecting for Certified Reference Materials (Langfang, P. R. China). Certified reference material of W-2a diabase (Al, 15.45%; Fe, 10.83%) was purchased from the United States Geological Survey (USGS, USA). Other mineral samples were provided by the Technical Center for Industrial Product and Raw Material Inspection and Testing, Shanghai Customs (Shanghai, P. R. China). $PM_{3.3\text{-}10}$ and rain water were collected at the Chemistry Building on Xianlin Campus of Nanjing University. River water was taken from the Yangtze River in Nanjing. All water samples were filtered through a 0.45 μm cellulose acetate membrane before analysis. The $PM_{3.3\text{-}10}$, soil, sediment, coal and ore samples were digested with hydrogen peroxide and aqua regia before analysis.[36] The detailed procedure is given in Supplementary Material.

**Apparatus.** The determination of cerium was performed on a PerkinElmer NexION 350D ICP-MS (PerkinElmer, Inc., USA) and the optimum operating conditions are summarized in Table S1. The pH values of the solutions were measured with a Mettler-Toledo Five Easy Plus pH meter (Shanghai, P. R. China). Scanning electron microscopy (SEM) images of materials were taken on a Hitachi S-3400N II electron microscope (Tokyo, Japan). Energy-dispersive X-ray spectroscopy (EDX) was carried out with an EX 250 spectroscope (Horiba, Kyoto, Japan) attached to the S-3400N II SEM. Transmission electron microscopy (TEM) images were obtained on a JEOL JEM-200CX microscope (Tokyo, Japan) operated at 200 kV. The X-ray diffraction (XRD) patterns were collected on a Bruker D8 Advance X-ray powder diffractometer (Bruker, Germany) with Cu Kα radiation operated at tube voltage and current of 40 kV and 40 mA, respectively. Thermogravimetric analysis (TGA) was studied on a STA-499C thermal analyzer (Netzsch, Germany) at a heating rate of 10 °C $min^{-1}$ from 25 to 800 °C in air. Fourier-transform infrared (FT-IR) spectra of materials were recorded on a Nicolet-6700 spectrometer (USA) using the KBr pellet technique. The magnetism measurement was performed using a superconducting quantum interference device (SQUID) magnetometer (Quantum Design, USA) at room temperature.

**Preparation of Ce(III)-MIIP.** The preparation of $Fe_3O_4$@HM nanocomposites is referred to in our previous work.[35] The detailed procedure is given in Supplementary Material. The Ce(III) ion imprinted polymer grafted $Fe_3O_4$@HM was prepared by using the surface ion imprinting technology via free radical polymerization reaction.[37, 38] In detail, $Ce(NO_3)_3·6H_2O$ (43.4 mg) and AM (28.4 mg) were dissolved in a 100-mL mixture solution of $CH_3OH/H_2O$ (4:1, v/v). Then, $Fe_3O_4$@HM (0.8 g), EGDMA (800 μL) and AIBN (30 mg) were added to the mixture, stirred for 10 min and transferred to a 200-mL flask. Then the reaction was initiated at 70 °C in an oil bath and maintained at that temperature for 16 h. The obtained product was collected with a magnet and washed with 1.0 mol·$L^{-1}$ HCl several times to remove Ce(III) until no cerium ion was detected in the supernatant by ICP-MS, and finally dried under vacuum at 60 °C overnight. The magnetic non-imprinted polymer (Ce(III)-MNIP) was also synthesized following the same procedure but without adding Ce(III) ions. The schematic of the synthesis from $Fe_3O_4$ to Ce(III)-MIIP is illustrated in Fig. 1.

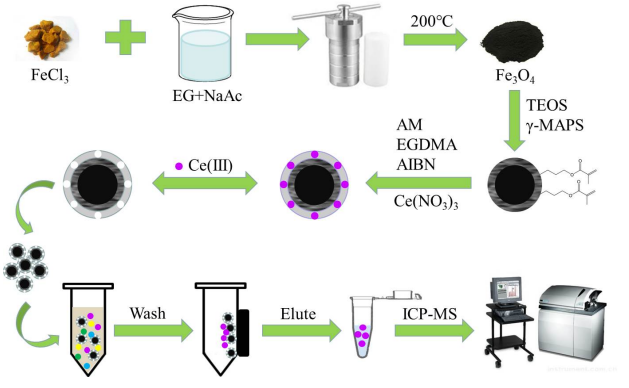


**Fig. 1** Schematic diagram of the procedure for preparation of Ce(III)-MIIP and MSPE of cerium ion.

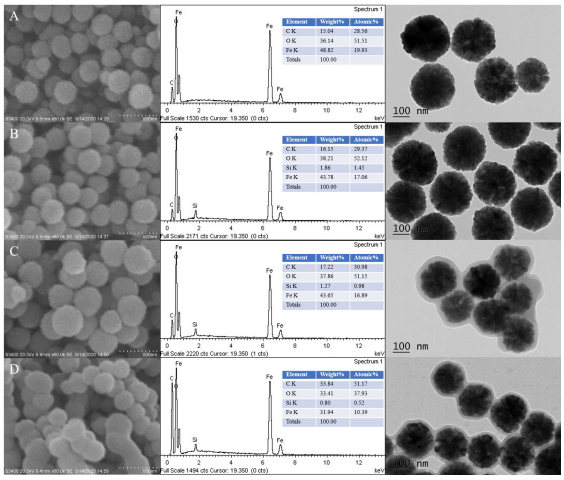

**Fig. 2** SEM images (left), EDX spectra (middle) and TEM images (right) of $Fe_3O_4$ (A), $Fe_3O_4$@HM (B), Ce(III)-MIIP (C) and Ce(III)-MNIP (D). Scale bar of SEM images: 500 nm; scale bar of TEM images: 100 nm.

**Extraction procedure.** The MSPE procedure for enrichment of cerium ions is shown in Fig. 1. In the adsorption step, the pH of 50 mL aqueous solution containing Ce(III) was adjusted to 6.0 by adding HCl or $NH_3 \cdot H_2O$ solution. Then 10 mg of Ce(III)-MIIP nanocomposites were added to the sample solution as MSPE adsorbent. After this solution was stirred for 15 min to obtain adsorption equilibrium, the Ce(III) loaded Ce(III)-MIIP adsorbent was isolated using a magnet. In the desorption step, the Ce(III) on the adsorbent was eluted with 2.0 mL 1.0 $mol \cdot L^{-1}$ HCl under continuous stirring. After achieving desorption equilibrium, the concentration of Ce(III) was determined by ICP-MS.

## RESULTS AND DISCUSSION

**Characterization.** The surface morphology, size and composition analysis of $Fe_3O_4$, $Fe_3O_4$@HM, Ce(III)-MIIP and Ce(III)-MNIP were characterized by SEM, EDX and TEM. Fig. 2 shows the SEM images, EDX spectra and TEM images of the $Fe_3O_4$, $Fe_3O_4$@HM, Ce(III)-MIIP and Ce(III)-MNIP. As shown in the SEM images, the average diameters of the $Fe_3O_4$ nanospheres were 200 nm. The particle size of $Fe_3O_4$@HM was slightly increased compared to $Fe_3O_4$, which was due to the encapsulation of the hybrid monolithic material. The particle size of Ce(III)-MIIP increased to about 250 nm and was slightly larger than that of Ce(III)-MNIP. This was due to the presence of imprinted holes in the imprinted layer, which made the surface of the material looser. The results from the EDX spectra showed that the Ce(III)-MIIP contains C, O, Si and Fe, indicating that the ion-imprinted layer was generated by stepwise polymerization. The TEM images further confirmed that the prepared materials were uniform, quasi-spherical in shape, and had nearly uniform distribution of particle size. As the TEM images of Ce(III)-MIIP and Ce(III)-MNIP showed, due to the free radical polymerization reaction during the imprinting process, the core-shell structured $Fe_3O_4$@HM nanocomposites were wrapped around a translucent polymer layer with a thickness of about 50 nm.

The FT-IR spectra of the $Fe_3O_4$, $Fe_3O_4$@HM, Ce(III)-MIIP and Ce(III)-MNIP are shown in Fig. 3A. The characteristic peak at 578 $cm^{-1}$, corresponding to the stretching of the Fe-O bond, was observed in all spectra. The characteristic peaks of Si-O, C=C and C=O at 1120, 1635 and 1720 $cm^{-1}$, respectively, were observed in the spectrum of $Fe_3O_4$@HM. The peak at 1452 $cm^{-1}$ in the spectra of Ce(III)-MIIP and Ce(III)-MNIP was ascribed to the characteristic absorption of C-N from the functional monomer AM. The remarkable rise of the intensities of the C=C and C=O peaks came from AM and EGDMA. And the peak of 2960 $cm^{-1}$ was assigned to the stretching vibration of the C-H bond, which was attributed to the formation of organics in the imprinted layer. These results confirmed the successful preparation of the $Fe_3O_4$, $Fe_3O_4$@HM, Ce(III)-MIIP and Ce(III)-MNIP.

The XRD patterns of $Fe_3O_4$, $Fe_3O_4$@HM, Ce(III)-MIIP and Ce(III)-MNIP are shown in Fig. 3B. Six main peaks were observed in four materials at the indices of (220), (311), (400), (422), (511) and (440), which corresponded to the standard XRD data card of the $Fe_3O_4$ crystal (JCPDS No. 19-0629). In comparison to $Fe_3O_4$, the peak intensity of $Fe_3O_4$@HM was weakened, indicating that the hybrid monolith was successfully coated on $Fe_3O_4$. And compared with $Fe_3O_4$@HM, each peak intensity of the Ce(III)-MIIP and Ce(III)-MNIP was weakened with the peak position unchanged, suggesting that the polymer was successfully grafted on $Fe_3O_4$@HM and did not change the crystal structure of $Fe_3O_4$. All of the results indicated that the crystal phase of the $Fe_3O_4$ nanoparticles was not changed upon coating of the hybrid monolith and ion imprinting polymerization process.

To analyze the thermal stability and content of the prepared materials, $Fe_3O_4$, $Fe_3O_4$@HM, Ce(III)-MIIP and Ce(III)-MNIP were characterized using thermogravimetric analysis, the results are shown in Fig. 3C. The weight loss of the four materials was slight at 30-160 °C, which was due to the evaporation of adsorbed water and residual solvents on the surface of the materials. For the TGA curve of the $Fe_3O_4$ nanoparticles, the weight loss of 3.2% at 550-600 °C was ascribed to the transformation of $Fe_3O_4$ to α-$Fe_2O_3$. Due to the coating of hybrid monolithic material, the same transformation for $Fe_3O_4$@HM occurred at a higher temperature in the range of 620-700 °C. And in the range of 400-620 °C, the slight weight loss was ascribed to the slow decomposition of hybrid monolithic material, indicating its great stability. The weight loss trend of Ce(III)-MIIP was the same with Ce(III)-MNIP due to the similar preparation process. The weight loss occurred from 280 to 450 °C, owing to the decomposition of organic matter in the imprinted layer of the outermost shell. The next flatter stage occurred between 450 to 700 °C, which can be explained by the decomposition of the hybrid monolithic material wrapped on the surface of $Fe_3O_4$. The last stage occurred in the range of 700 to

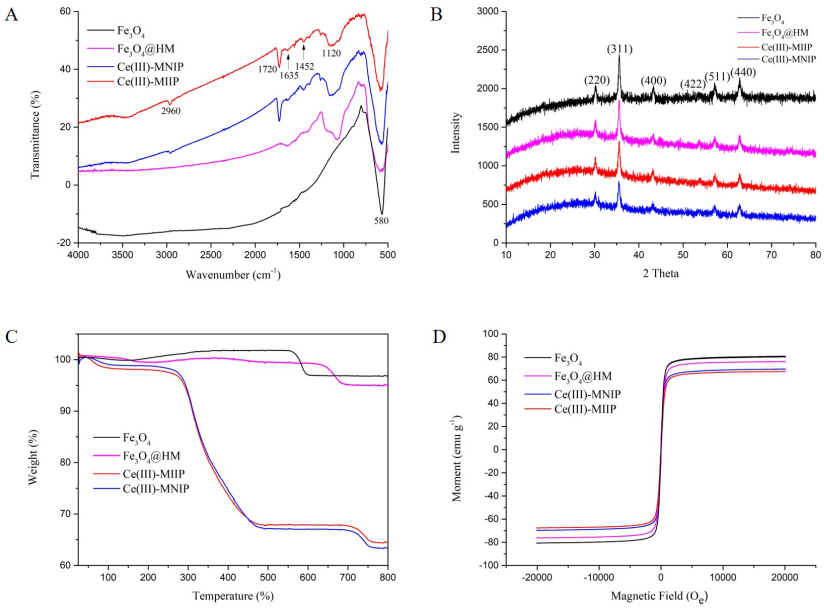


**Fig. 3** FT-IR spectra (A), XRD patterns (B), TGA curves (C) and magnetization curves (D) of $Fe_3O_4$, $Fe_3O_4$@HM, Ce(III)-MIIP and Ce(III)-MNIP.

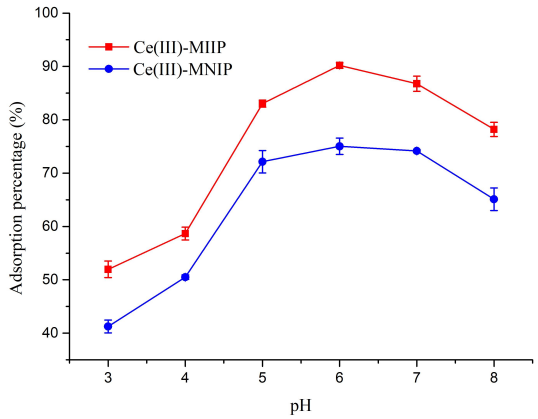


**Fig. 4** Influence of solution pH on adsorption rate of Ce(III) onto Ce(III)-MIIP and Ce(III)-MNIP. Dose of adsorbent: 10 mg; concentration of Ce(III): 20 μg·$L^{-1}$; sample volume: 50 mL; extraction time: 15 min.

750 °C, which corresponded to the transformation of $Fe_3O_4$ to α-$Fe_2O_3$. The total weight loss of the Ce(III)-MIIP and Ce(III)-MNIP nanocomposites was 35.6% and 36.7%, respectively.

To study the effect of magnetism on the separation process, the magnetization curves of the materials were prepared. The magnetic hysteresis loops of the $Fe_3O_4$, $Fe_3O_4$@HM, Ce(III)-MIIP and Ce(III)-MNIP nanocomposites are displayed in Fig. 3D. Their saturation magnetization values were 80.2, 76.1, 67.5 and 69.6 emu·$g^{-1}$, respectively. The slight decrease of saturation magnetization of the $Fe_3O_4$@HM nanocomposites compared to $Fe_3O_4$ was observed owing to the nonmagnetic hybrid monolithic material wrapped on the surface of $Fe_3O_4$. The significant decrease on saturation magnetization of Ce(III)-MIIP and Ce(III)-MNIP was attributed to the coating of the nonmagnetic ion imprinted polymer. In addition, the weaker magnetism of Ce(III)-MIIP than Ce(III)-MNIP was attributed to the formation of more abundant imprinted cavities based on the much larger surface area, as reported by the Hu research group.[39] The final magnetism was sufficient for Ce(III)-MIIP to be separated with a magnet.

## Optimization studies

**Effect of loading condition on adsorption.** The effect of pH on the adsorption process is very crucial because the pH of the aqueous solutions can influence both the ionic stability and the number of the protonated functional groups of the polymer. In this work, the effect of pH on the Ce(III)-MIIP adsorption percentage was examined by adjusting the pH of the solution in the range of pH 3.0-8.0. As indicated in Fig. 4, with the pH value increasing between 3.0 to 6.0, the adsorption ability increased greatly and reached a maximum at pH 6.0. However, the adsorption rate decreased when the pH continued to increase. This could be explained that at a lower pH, the electrostatic repulsion force between the Ce(III) ions and the positively charged surface of the adsorbent, which was created by protonation of the amino groups, became stronger, leading to a lower adsorption rate. As the pH increased, the functional monomer gradually deprotonated, so that the adsorption efficiency increased and reached maximum value when the pH was 6.0. When the pH was above 6.0, precipitation of the cerium hydroxide could occur, which would reduce the adsorption of Ce(III) on Ce(III)-MIIP. Therefore, the sample pH of 6.0 was selected for adsorbing Ce(III) in subsequent experiments.

In order to investigate the effect of contact time on the adsorption rate of Ce(III) onto Ce(III)-MIIP, the adsorption kinetics was evaluated in a time interval between 1 and 30 min; the results are shown in Fig. S1. The adsorption rate of Ce(III)-MIIP increased rapidly during the first 5 min, then plateaued at 15 min and reached equilibrium. In the initial stage of adsorption,

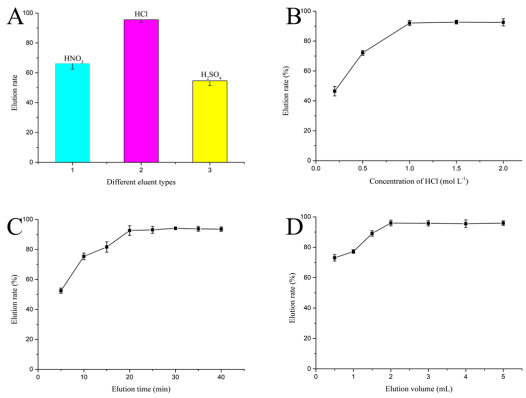


**Fig. 5** Effect of type of eluent (A), concentration of HCl (B), elution time (C) and volume (D) on elution rate of Ce(III) from Ce(III)-MIIP. Dose of adsorbent: 10 mg; solution pH: 6.0; concentration of Ce(III): 20 μg·L$^{-1}$; sample volume: 50 mL; extraction time: 15 min. Elution conditions: eluent: A. 5 mL 1 mol·L$^{-1}$ $HNO_3$, HCl and $H_2SO_4$; B. 2 mL HCl (0.2-2.0 mol·L$^{-1}$); C. 2 mL 1 mol·L$^{-1}$ HCl; D. 1 mol·L$^{-1}$ HCl (0.5-5 mL); elution time: A: 20 min; B: 20 min; C: 5-40 min; D: 20 min.

large numbers of imprinting sites were available on the surface of the adsorbent, so the adsorption was relatively quick. Over time, the number of imprinting sites on the polymer surface that remained unoccupied by Ce(III) gradually decreased. Therefore, the increase of the amount of adsorbed Ce(III) continually slowed, and finally the adsorption essentially reached saturation. In subsequent experiments, 15 min was selected.

In the analysis of real samples, the sample volume is one of the important parameters influencing the preconcentration factor. Therefore, the effect of sample volume on the quantitative adsorption of the Ce(III) ions was investigated (Fig. S2). For this purpose, 10 mg of Ce(III)-MIIP was suspended in different sample volumes (10, 30, 50, 70, 90, 100 mL) and the total amount of loaded Ce(III) was kept constant at 50 ng. When the sample volume was less than 100 mL, the adsorption rate of Ce(III) was greater than 90%. Comprehensively considering the experimental efficiency and the experimental time, we chose 50 mL as the sample volume for subsequent experiments. If the cost of time does not need to be considered, a higher concentration multiple could be obtained by increasing the sample volume.

**Effect of elution condition on desorption.** It can be seen from the results of the sample pH experiment that Ce(III) was hardly adsorbed on Ce(III)-MIIP under strong acid condition. Based on this, the reported HCl[28] and other acid reagents, $HNO_3$ and $H_2SO_4$ were selected as the eluents to release the adsorbed Ce(III) from Ce(III)-MIIP. As shown in Fig. 5A, HCl had the best elution effect with the same elution conditions (concentration, 1.0 mol·L$^{-1}$; volume, 5 mL). Then, the effect of the concentration of HCl on the elution rate was investigated (Fig. 5B). The maximum elution rate was achieved when the concentration of HCl reached 1.0 mol·L$^{-1}$. The effect of elution time on the elution rate of Ce(III) was investigated in the range of 5-40 min. It was found that the elution rate increased up to 90% when the desorption time was 20 min (Fig. 5C). The effect of eluent volume was also optimized in the range of 0.5-5 mL, and from Fig. 5D it can be seen that 2.0 mL of the eluent was plentiful for desorbing the target ions from Ce(III)-MIIP. Considering the enrichment factor, the eluent being as low as possible, the elution volume was ultimately set to 2.0 mL when the sample volume was 50 mL with an enrichment of 25 times for the cerium ions.

**The adsorption capacity.** The adsorption capacity is an important factor for evaluating Ce(III)-MIIP and Ce(III)-MNIP. It is defined as the maximum amount of metal ions per gram of sorbent. The adsorption capacity ($Q_e$, mg·g$^{-1}$) and the adsorption amount at $t$ min ($Q_t$, mg·g$^{-1}$) were calculated with the following equations:

$$Q_e = \frac{C_0 - C_e}{m} \times V$$

$$Q_t = \frac{C_0 - C_t}{m} \times V$$

where $C_0$, $C_t$ and $C_e$ are the initial concentration of Ce(III), concentration of Ce(III) at $t$ min, and the final concentration of Ce(III) under equilibrium, respectively. $V$ is the volume of the solution (L), and $m$ is the amount of the adsorbent (g).

The isothermal adsorption curves of Ce(III)-MIIP and Ce(III)-MNIP provide important information on the process of Ce(III) adsorption by these materials. To investigate this parameter, Ce(III)-MIIP or Ce(III)-MNIP (10 mg) were equilibrated with Ce(III) solutions (50 mL) with different initial concentrations of 1, 5, 10, 20, 30, 40 mg·L$^{-1}$ at pH 6.0. As can be seen in Fig. S3, when the Ce(III) concentration increased, the adsorption amount first increased sharply, then increased slightly, and finally reached saturation. The adsorption capacities of Ce(III)-MIIP and Ce(III)-MNIP were calculated to be 67.8 and 27.4 mg·g$^{-1}$, respectively. The capacity of Ce(III)-MIIP was larger than that of Ce(III)-MNIP. This difference indicated that imprinting played an important role in the adsorbent behavior. During preparation of the Ce(III)-MIIP, the presence of Ce(III) encouraged an orderly ligand arrangement. After removal of Ce(III), the imprinted cavities and specific binding sites of the functional groups in a predetermined orientation were formed. However, no such specificity was found in Ce(III)-MNIP. Therefore, the memory effect owned by Ce(III)-MIIP to the Ce(III) ions allowed it to possess a higher adsorption capacity to the metal ions than Ce(III)-MNIP.

The adsorption behaviors of Ce(III)-MIIP and Ce(III)-MNIP were studied to determine the adsorption mechanism. Langmuir and Freundlich adsorption isotherm models were used to fit the adsorption process in this study. These models are defined by the following two equations:

Langmuir isotherm model:

$$\frac{C_e}{q_e} = \frac{C_e}{q_m} + \frac{1}{q_m K_L}$$

**Table 1 Distribution Ratio ($K_d$), Selectivity Coefficient ($K$) and Relative Selectivity Coefficient ($K'$) Values of Ce(III)-MIIP and Ce(III)-MNIP Mate**

| Cation | $K_d$ | | $K$ | | $K'$ |
|---|---|---|---|---|---|
| | MIIP | MNIP | MIIP | MNIP | |
| **Ce(III)** | 57.89 | 6.27 | - | - | - |
| **Fe(III)** | 0.55 | 2.77 | 106.01 | 2.27 | 46.78 |
| **Pb(II)** | 0.60 | 2.32 | 96.03 | 2.71 | 35.47 |
| **Ca(II)** | 0.60 | 2.40 | 97.05 | 2.61 | 37.16 |
| **Ag(I)** | 0.52 | 2.81 | 111.89 | 2.23 | 50.14 |

Freundlich isotherm model:

$$\ln q_e = \frac{\ln C_e}{n} + \ln K_F$$

where $q_m$ (mg·g$^{-1}$) is the maximum adsorption capacity at equilibrium; $C_e$ (mg·L$^{-1}$) and $q_e$ (mg·g$^{-1}$) represent the equilibrium concentration and adsorption capacity towards Ce(III) in solution at adsorption equilibrium, respectively; $K_L$ (L·mg$^{-1}$) is the Langmuir constant, which is related to the affinity between the adsorbent and the solution. $K_F$ (mg·g$^{-1}$) and $n$ (Freundlich constants) indicate the adsorption capacity and adsorption intensity, respectively.

Fitting of the experimental data to the adsorption model was performed. The curves are shown in Fig. S4 and the corresponding isotherm constants are summarized in Table S2. The correlation coefficients of Ce(III)-MIIP and Ce(III)-MNIP for the Langmuir model (0.971 and 0.994, respectively) were better than those for the Freundlich model (0.917 and 0.968, respectively) in describing the adsorption process, indicating that the binding sites of Ce(III)-MIIP and Ce(III)-MNIP were uniformly distributed on their surfaces and the adsorption process tended to be monolayer adsorption.

**Selectivity study.** The adsorption selectivity of Ce(III)-MIIP and Ce(III)-MNIP was investigated in the mixture containing competitive ions. Four types of metal ions, Fe(III), Pb(II), Ca(II) and Ag(I), were selected as competitors, which have the same charge or similar ionic radius as Ce(III). Their ionic radii are 64 pm, 119 pm, 100 pm and 94 pm for Fe(III), Pb(II), Ca(II) and Ag(I), respectively, which are close to 102 pm for Ce(III). 10 mg of Ce(III)-MIIP and Ce(III)-MNIP was added into 50 mL of mixed solution containing 20 μg·L$^{-1}$ of each metal ion mentioned above. After reaching adsorption equilibrium, the concentrations of each type of ion were determined. The distribution coefficient $K_d$, selective coefficient $K$ and relative selectivity coefficient $K'$ were calculated according to the formulas below. The results are shown in Table 1.

$$K_d = \frac{C_0 - C_e}{C_e} \times \frac{V}{m}$$

$$K = \frac{K_{d-template\ metal}}{K_{d-interferent\ metal}}$$

$$K' = \frac{K_{IIP}}{K_{NIP}}$$

where $C_0$ and $C_e$ represent the concentrations of given metal ions in the initial and equilibrated solutions, respectively. $V$ is the volume of the solution and $m$ is the weight of the adsorbent.

As can be seen in Table 1, Ce(III)-MIIP exhibited good adsorption selectivity for Ce(III) in the presence of the competitive metal ions. The adsorption ability for the four competing metal ions was lower compared to that for Ce(III), which could be attributed to the imprinting effect. The relative selectivity coefficients of Ce(III)-MIIP for Ce(III)/Fe(III), Ce(III)/Pb(II), Ce(III)/Ca(II) and Ce(III)/Ag(I) were further calculated to be 46.78, 35.47, 37.16 and 50.14 times higher than those of Ce(III)-MNIP, respectively. This can be interpreted that selective binding sites towards Ce(III) were effectively formed in the Ce(III)-MIIP. It is clear that the polymer recognized the template Ce(III) preferentially, and this demonstrated the successful formation of the imprinted cavities and the significance of the memory effect of Ce(III)-MIIP.

**Interference study.** The interference of other main coexisting ions in environmental and mineral samples includes $Al^{3+}$, $Na^+$, $K^+$, $Fe^{3+}$, $Mg^{2+}$, $NO^{3-}$, $Cl^-$, and $SO_4^{2-}$, *etc.* The determination of Ce(III) was examined using a 50 mL solution containing 5 μg·L$^{-1}$ target Ce(III) ions and a certain concentration of interfering ions as the sample under the optimized conditions described above. The results in Table S3 indicate that in the presence of 20 mg·L$^{-1}$ $Al^{3+}$, $Na^+$, $K^+$, $NO^{3-}$ and $Cl^-$, 10 mg·L$^{-1}$ $Fe^{3+}$, $Mg^{2+}$, $Ca^{2+}$ and $SO_4^{2-}$, the recoveries of Ce(III) were still in the range of 92.4-104.0%. Therefore, the proposed method could be applied for the analysis of Ce(III) in real samples with good tolerance of interference.

**Reusability.** Reusability is one of the important advantages of a novel adsorbent. To investigate the stability and reusability of the Ce(III)-MIIP, it was washed with 1 mol·L$^{-1}$ HCl eluent and then reused to adsorb Ce(III). We performed 15 consecutive adsorption/desorption cycles with the same MIIP adsorbent. As can be seen from the Fig. 6, the recovery of Ce(III) on Ce(III)-

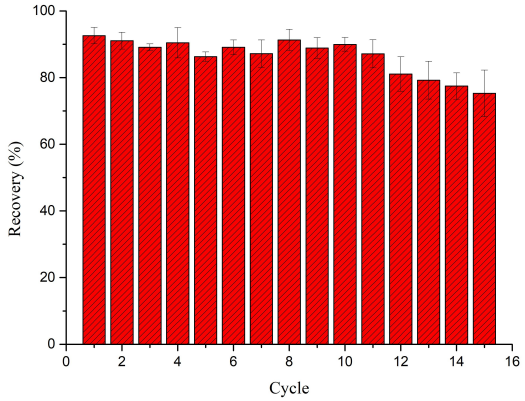


**Fig. 6** Reusability of Ce(III)-MIIP. MSPE conditions: Dose of adsorbent: 10 mg; solution pH: 6.0; concentration of Ce(III): 20 μg·L$^{-1}$; sample volume: 50 mL; extraction time: 15 min; elution condition: eluent: 2.0 mL 1 mol·L$^{-1}$ HCl; elution time: 20 min.

**Table 2 Analytical Results of Ce in Certified Reference Materials (mean ± SD, n=3)**

| Certified Reference Material | Found | Reference value | Recovery (%) |
|---|---|---|---|
| | ($g\ t^{-1}$) | | |
| **GSS-3** | 36.50±1.21 | 39 | 93.6 |
| **GSD-10** | 36.35±2.08 | 38 | 95.6 |
| **W-2a** | 20.85±0.64 | 23 | 90.7 |

MIIP particles did not show an obvious decrease after reusing the same Ce(III)-MIIP for 12 times, with the recovery of Ce(III) above 80%. However, it gradually decreased to 75% after the adsorbent was used repeatedly for 15 times. The results indicated that Ce(III)-MIIP had good stability and could maintain good retention without any obvious loss after being repeatedly used 12 times.

**Analytical performance.** With the overall optimized conditions, the advantages of the MSPE-ICP-MS protocol for Ce(III) determination were evaluated. The limit of detection (LOD, defined as 3-fold signal-to-noise ratio) was 0.008 $\mu g \cdot L^{-1}$ for Ce(III), and the limit of quantification (defined as 10-fold signal-to-noise ratio) for Ce(III) was 0.05 $\mu g \cdot L^{-1}$. The calibration curve in this work was established in the range of 0.05-50 $\mu g \cdot L^{-1}$ Ce(III) with a linear equation of $y = 24.018\ x + 5.8654$, and a linear correlation coefficient above 0.9986. Therefore, this protocol is quite suitable for cerium analysis of environmental and mineral samples.

**Sample analysis.** The accuracy of the proposed method was verified by determining cerium in the certified reference materials GSS-3 (Soil), GSD-10 (Sediment) and W-2a (Diabase). The results as summarized in Table 2 indicate that the determined values of the quantities of cerium were in accordance with the certified values, which further proved the reliability of this protocol. In addition, the analytical results for the resulting supernatant of W-2a after treatment with the prepared Ce(III)-MIIP by ICP-OES (PerkinElmer, Inc., Optima 5300, USA) showed that 75.4% Al(III) and 86.8% Fe(III) were eliminated by the MSPE procedure. The concentrations of both dominant matrix ions decreased below their tolerance levels for Ce(III) determination. Consequently, this Ce(III)-MIIP adsorbent could not only realize high selective enrichment of target cerium ions, but also effectively eliminate the interference of major metals in corresponding ores.

Furthermore, environmental water, $PM_{3.3\text{-}10}$, coal and ore samples were used for assessing the feasibility of the protocol developed in this work. As listed in Table S4, the analytical accuracy was further evaluated by spiking known amounts of standard cerium ions in these real samples. The recoveries of Ce(III) in all spiked samples were obtained at 86.9%-114.9%. The experimental results indicate that this proposed method could be applied for the determination of cerium in real environmental and mineral samples.

**Comparison with other adsorbents.** Some parameters of the published methods using an ion-imprinted polymer as the adsorbent for Ce(III) are summarized in Table 3.[28, 32-34] As is shown, the Ce(III)-MIIP nanocomposite prepared in this work presented comparable adsorption capacity and enrichment factor, as well as competitive adsorption time, reusability and relative standard deviations (RSDs). Notably, among all the listed methods, our method exhibited the highest sensitivity. Considering all the above parameters, it can be seen that Ce(III)-MIIP could be a good potential candidate for extraction of Ce(III) from environment and mineral samples.

## CONCLUSIONS

A highly efficient Ce(III)-MIIP nanocomposite, grafted on vinyl functionalized organic-inorganic hybrid monolith decorated $Fe_3O_4$, was successfully synthesized via the surface ion imprinting technique. The core of $Fe_3O_4$ nanoparticles prepared by the solvothermal method was uniformly dispersed and uniform in size. Moreover, the formation of a hybrid monolithic interlayer endowed the resultant Ce(III)-MIIP with stable chemical property and firmly rigid configuration. The Ce(III) ions could be captured by Ce(III)-MIIP at pH 6.0 and quantitatively eluted with 1 $mol \cdot L^{-1}$ HCl in MSPE operation. The obtained Ce(III)-MIIP exhibited a very high degree of selectivity and adsorption ability towards the Ce(III) ions owing to the specific cavities based on the coordination interaction between functional monomer (AM) and template metal ions (cerium ions). The maximum adsorption capacity of Ce(III)-MIIP was 67.8 $mg \cdot g^{-1}$ with a fast adsorption

**Table 3 Comparison with Other Published Works**

| Functional monomer | Preparation technique | Adsorption capacity (mg $g^{-1}$) | Enrichment factor | Adsorption time (min) | Reusability | Detection technique | LOD (μg $L^{-1}$) | RSD (%) | Ref. |
|---|---|---|---|---|---|---|---|---|---|
| **2-Hydroxyethyl methacrylate and N-methacryloylamido antipyrine** | Bulk polymerization | 36.58 | - | 30 | 25 | ICP-MS | 50 | - | 28 |
| **Chitosan** | Surface-imprinting | 43 | 100 | 13 | 6 | ICP-AES | 0.037 | 5.1 | 32 |
| **Chitosan** | | 130.55 | 20 | 8 | 4 | | 0.057 | < 2.6 | 33 |
| **Acrylamide** | | 87.42 | - | 45 | - | | - | - | 34 |
| **Acrylamide** | | 67.8 | 25 | 15 | 12 | ICP-MS | 0.008 | 1.7-7.0 | This work |

rate. To the best of our knowledge, this work is the first attempt at using a magnetic ion imprinted polymer based on hybrid monolith decorated $Fe_3O_4$ nanoparticles as a satisfactory MSPE sorbent, combined with ICP-MS determination of cerium in complex environmental and mineral samples, especially in ores with a high concentration of the main metal.

## ASSOCIATED CONTENT

Please contact the corresponding author for the Supporting Information (Fig S1-S4 and Table S1-S4).

## AUTHOR INFORMATION


**Corresponding Author**

* H. Z. Lian

Email address: hzlian@nju.edu.cn

* S. Liu

Email address: liu_shu@customs.gov.cn


**Notes**

The authors declare no competing financial interest.

## ACKNOWLEDGMENTS


This work was supported by the National Key R&D Program of China (2018YFF0215400), the National Natural Science Foundation of China (21874065, 91643105, and 21577057), the Natural Science Foundation of Jiangsu Province (BK20171335), and the Scientific Research Projects of the General Administration of Customs (2019HK074).


## REFERENCES


1. T. Pasinli, A. E. Eroglo, and T. Shahwan, *Anal. Chim. Acta*, 2005, **547**, 42-49. https://doi.org/10.1016/j.aca.2005.04.076
2. R. M. Ashour, A. F. Abdel-Magied, A. A. Abdel-khalek, O. S. Helaly, and M. M. Ali, *J. Environ. Chem. Eng.*, 2016, **4**, 3114-3121. https://doi.org/10.1016/j.jece.2016.06.022
3. L. Y. Zhu, X. Q. Wang, G. Yu, X. Q. Hou, G. H. Zhang, J. Sun, X. J. Liu, and D. Xu, *Mater. Res. Bull.*, 2008, **43**, 1032-1037. https://doi.org/10.1016/j.materresbull.2007.04.025
4. Q. Zhang, K. Ge, J. L. Duan, R. Zhang, C. M. Zhang, S. X. Wang, and J. C. Zhang, *J. Nanopar. Res.*, 2014, **16**, 2697. https://doi.org/10.1007/s11051-014-2697-3
5. P. Sahu, S. Eniyarppu, M. Ahmed, D. Sharma, and A. Sakthivel, *J. Porous Mater.*, 2018, **25**, 999-1005. https://doi.org/10.1007/s10934-017-0510-2
6. Z. H. Zhang and R. Balasubramanian, *Environ. Sci. Technol.*, 2017, **51**, 4248-4258. https://doi.org/10.1021/acs.est.7b00920
7. R. Kechiched, R. Laouar, O, Bruguier, L. Kocsis, S. Salmi-Laouar, D. Bosch, O. Ameur-Zaimeche, A. Foufou, and H. Larit, *J. Geochem. Explor.*, 2020, **208**, 106396. https://doi.org/10.1016/j.gexplo.2019.106396
8. E. H. El-Araby, M. Abd El-Wahab, H. M. Diab, T. M. El-Desouky, and M. Mohsen, *Appl. Radiat. Isotopes*, 2011, **69**, 1506-1511. https://doi.org/10.1016/j.apradiso.2011.06.005
9. T. A. Stueckle, D. C. Davidson, R. Derk, T. G. Kornberg, D. Schwegler-Berry, S. V. Pirela, G. Deloid, P. Demokritou, S. Luanpitpong, Y. Rojanasakul, and L. Y. Wang, *NanoImpact*, 2017, **6**, 39-54. https://doi.org/10.1016/j.impact.2016.11.001
10. A. P. Packer, D. Lariviere, C. S. Li, M. Chen, A. Fawcett, K. Nielsen, K. Mattson, A. Chatt, C. Scriver, and L. S. Erhardt, *Anal. Chim. Acta*, 2007, **588**, 166-172. https://doi.org/10.1016/j.aca.2007.02.024
11. F. F. Hu, C. H. Wang, and J. D. Li, *J. Chin. Mass Spectr. Soc.*, 2014, **35**, 330-334. https://doi.org/10.7538/zpxb.youxian.2014.0014
12. H. Sereshti, A. R. Far, and S. Samadi, *Anal. Lett.*, 2012, **45**, 1426-1439. https://doi.org/10.1080/00032719.2012.675490
13. J. C. Farinas, I. Rucandio, M. S. Pomares-Alfonso, M. E. Villanueva-Tagle, and M. T. Larrea, *Talanta*, 2016, **154**, 53-62. https://doi.org/10.1016/j.talanta.2016.03.047
14. P. Zuzaan, N. Gansukh, and D. Bolortuya, *X-Ray Spectrom.*, 2010, **39**, 52-56. https://doi.org/10.1002/xrs.1221
15. D. Suvorova, E. Khudonogova, and A. Revenko, *X-Ray Spectrom.*, 2017, **46**, 200-208. https://doi.org/10.1002/xrs.2747
16. A. T. Kashuba and C. R. Hines, *Anal. Chem.*, 1971, **43**, 1758-1761. https://doi.org/10.1021/ac60307a003
17. I. M. Issa, R. M. Issa, and Y. Z. Ahmed, *Microchem. J.*, 1973, **18**, 569-576. https://doi.org/10.1016/0026-265X(73)90088-X
18. G. I. Malofeeva, O. M. Petrukhin, B. Y. Spivakov, and L. S. Rozhkova, *J. Anal. Chem.*, 2001, **56**, 238-242. https://doi.org/10.1023/A:1009450322031
19. S. Nishihama, T. Hirai, and I. Komasawa, *J. Solid State Chem.*, 2003, **171**, 101-108. https://doi.org/10.1016/S0022-4596(02)00198-6
20. J. P. Sun, Q. L. Liang, Q. Han, X. Q. Zhang, and M. Y. Ding, *Talanta*, 2015, **132**, 557-563. https://doi.org/10.1016/j.talanta.2014.09.043
21. L. M. Cui, Y. G. Wang, L. Gao, L. H. Hu, L. G. Yan, Q. Wei, and B. Du, *Chem. Eng. J.*, 2015, **281**, 1-10. https://doi.org/10.1016/j.cej.2015.06.043
22. M. Saraji and H. Yousefi, *J. Hazard. Mater.*, 2009, **167**, 1152-1157. https://doi.org/10.1016/j.jhazmat.2009.01.111
23. S. Daniel, R. S. Praveen, and T. P. Rao, *Anal. Chim. Acta*, 2006, **570**, 79-87. https://doi.org/10.1016/j.aca.2006.04.007
24. J. Y Cui, Z. P. Zhou, S. J. Liu, Y. F. Zhang, L. Yan, Q. Zhang, S. Zhou, Y. S. Yan, and C.X. Li, *New J. Chem.*, 2018, **42**, 14502-14509. https://doi.org/10.1039/c8nj03249a
25. C. Esen, M. Andac, N. Bereli, R. Say, E. Henden, and A. Denizli, *Mater. Sci. Eng. C-Mater.*, 2009, **29**, 2464-2470. https://doi.org/10.1016/j.msec.2009.07.012
26. J. Otero-Romani, A. Moreda-Pineiro, P. Bermejo-Barrera, and A. Martin-Esteban, *Anal. Chim. Acta*, 2008, **630**, 1-9. https://doi.org/10.1016/j.aca.2008.09.049

27. W. Meouche, K. Laatikainen, A. Margaillan, T. Silvonen, H. Siren, T. Sainio, I. Beurroies, R. Denoyel, and C. Branger, *Eur. Polym. J.*, 2017, **87**, 124-135. https://doi.org/10.1016/j.eurpolymj.2016.12.022
28. R. Keçili, İ. Dolak, B. Ziyadanoğulları, A. Ersöz, and R. Say *J. Rare Earths*, 2018, **36**, 857-862. https://doi.org/10.1016/j.jre.2018.02.008
29. M. L. Zhang, Z. H. Zhang, Y. N. Liu, X. Yang, L. J. Luo, J. T. Chen, and S. Z. Yao, *Chem. Eng. J.*, 2011, **178**, 443-450. https://doi.org/10.1016/j.cej.2011.10.035
30. Y. Liu, X. Hu, Z. C. Liu, M. J. Meng, J. M. Pan, Y. H. Jiang, L. Ni, and W. F. Wu, *Chem. Eng. J.*, 2017, **328**, 11-24. https://doi.org/10.1016/j.cej.2017.07.034
31. Z. C. Liu, W. F. Wu, Y. Liu, and X. Hu, *J. Taiwan Inst. Chem. Eng.*, 2018, **85**, 282-290. https://doi.org/10.1016/j.jtice.2018.02.001
32. X. J. Zhang, C. X. Li, Y. S. Yan, J. M. Pan, P. P. Xu, and X. H. Zhao, *Microchim. Acta*, 2010, **169**, 289-296. https://doi.org/10.1007/s00604-010-0352-y
33. J. M. Pan, X. H. Zou, C. X. Li, Y. Liu, Y. S. Yan, and J. Han, *Microchim. Acta*, 2010, **171**, 151-160. https://doi.org/10.1007/s00604-010-0416-z
34. Y. Liu, J. Qiu, Y. L. Jiang, Z. C. Liu, M. J. Meng, L. Ni, C. C. Qin, and J. B. Peng, *Micropor. Mesopor. Mater.*, 2016, **234**, 176-185. https://doi.org/10.1016/j.micromeso.2016.07.016
35. Y. Hua, J. Y. Li, H. Min, X. H. Wu, X. B. Cui, Y. J. Chen, H. Z. Lian, and D. Sheng, *Microchem. J.*, 2020, **158**, 105210. https://doi.org/10.1016/j.microc.2020.105210
36. E. S. Challaraj Emmanuel, V. Vignesh, B. Anandkumar, and S. Maruthamuthu, *Indian J. Microbiol.*, 2011, **51**, 488-495. https://doi.org/10.1007/s12088-011-0111-8
37. X. B. Luo, S. L. Luo, Y. C. Zhan, H. Y. Shu, Y. N. Huang, and X. M. Tu, *J. Hazard. Mater.*, 2011, **192**, 949-955. https://doi.org/10.1016/j.jhazmat.2011.05.042
38. Z. Y. Zhou, X. T. Liu, M. L. Zhang, J. Jiao, H. W. Zhang, J. Du, B. Zhang, and Z. Q. Ren, *Sci. Total Environ.*, 2020, **699**, 134334. https://doi.org/10.1016/j.scitotenv.2019.134334
39. B. S. Zhao, M. He, B. B. Chen, H. R. Xu, and B. Hu, *Spectrochim. Acta B*, 2018, **143**, 32-41. https://doi.org/10.1016/j.sab.2018.02.011